Growth promotion of Al-induced crystallized Ge films on insulators by insertion of a Ge membrane below the Al layer

著者別名	都甲 薫, 末益 崇
journal or publication title	Thin solid films
volume	557
page range	143-146
year	2014-04
権利	(C) 2013 Elsevier B.V. “NOTICE: this is the author’s version of a work that was accepted for publication in Thin Solid Films. Changes resulting from the publishing process, such as peer review, editing, corrections, structural formatting, and other quality control mechanisms may not be reflected in this document. Changes may have been made to this work since it was submitted for publication. A definitive version was subsequently published in Thin Solid Films,557,2014. http://dx.doi.org/10.1016/j.tsf.2013.08.040
URL	http://hdl.handle.net/2241/00121570

doi: 10.1016/j.tsf.2013.08.040

Growth promotion of Al-induced crystallized Ge films on insulators by insertion of a Ge membrane below the Al layer

Ryohei Numata[a], Kaoru Toko[a,*], Koki Nakazawa[a], Noritaka Usami[b], and Takashi Suemasu[a]

[a] *Institute of Applied Physics, University of Tsukuba, Tsukuba, Ibaraki 305-8573, Japan*

[b] *Materials, Phys. and Energy Eng., Nagoya Univ., Aichi 464-8603, Japan*

* Corresponding author: Kaoru Toko

Institute of Applied Physics, University of Tsukuba,

1-1-1 Tennohdai, Tsukuba, Ibaraki 305-8573, Japan

Phone: +81-29-853-5472, Fax: +81-29-853-5205

E-mail: toko@bk.tsukuba.ac.jp

Abstract

Al-induced crystallization (AIC) enables low-temperature crystallization of amorphous Ge thin films on insulators. We investigated growth promotion of Ge thin films using Ge membranes (1-10 nm thickness) that are initially inserted below the Al layer. These Ge insertion layers enhanced supersaturation of Al with Ge, which results in low-temperature AIC (275˚C). However, thick (≥ 3 nm) insertion layers result in small grains because of the high nucleation frequency. A 1-nm-thick insertion layer accomplished a growth promotion and yielded large grains of over 100 μm in diameter. Moreover, electron backscatter diffraction measurement revealed that the AIC-Ge layer was highly (111) oriented. This low-temperature crystallization technique opens up the possibility for developing Ge-based electronic devices on inexpensive glass substrates, as well as on flexible polymer substrates.

Keywords: A1.Crystal orientation, A2.Solid phase crystallization, B1.Polycrystalline films; B2.Semiconducting germanium

1. Introduction

Germanium is useful for fabricating high-speed metal-oxide-semiconductor field-effect transistors (MOSFETs) and high-efficiency tandem solar cells [1-3]. In particular, (111) oriented Ge provides the highest mobility for MOSFETs [1, 2], and is used as an epitaxial template for several advanced functional materials [4-6]. Because a bulk Ge substrate is extremely expensive, substituting the Ge substrate with a crystalline Ge (c-Ge) film on an inexpensive substrate, such as a glass or a polymer, is desired. In line with this, many researchers have investigated techniques for forming c-Ge films on insulators at low temperatures [7-14], because the softening temperature of the abovementioned substrates is low: approximately 550˚C for glasses and 300˚C for polymers. However, the resulting Ge layers consist of randomly oriented small grains (< 1 μm).

Study of Al-induced crystallization (AIC) of amorphous Si and Ge films on insulators has recently accelerated [15-28]. The AIC technique yields large-grained (diameters: 10-100 μm) polycrystalline Si films on insulators at low temperatures (420-550˚C) through exchange between the Al and Si layers [15-16]. The driving force behind the low-temperature crystallization in AIC-Si is the supersaturation of Al with Si atoms [15, 18]. In addition, the crystal orientation of the AIC-Si can be controlled to either (100) or (111), by modulating the growth conditions: the thickness of the Al and Si layers, the thickness of the interlayer between the Al and Si layers, and the annealing temperature [17-22].

The AIC technique enables the formation of polycrystalline Ge (poly-Ge) films on insulators at low temperatures (< 250˚C) [23-28]. However, the AIC-Ge films result in Ge-Al mixed structures composed of small grains (< 100 nm) [23-28] because of an the absence of layer exchange. Kurosawa *et al*. achieved a layer exchange growth in AIC of Ge at an annealing temperature of 410˚C, which resulted in relatively large grains (approx. 5 μm) with (111) orientation (70-% area fraction) [29]. Recently, we accomplished highly (111) oriented Ge films with large grains (>100 μm) by optimizing the interfacial AlO_x formation process and the annealing conditions (325˚C, 100 h) [30, 31]. If the annealing temperature can be reduced to below 300˚C, certain flexible polymer sheets can be used as a substrate. In line with this, we developed a growth promotion technique for AIC-Ge where a Ge membrane is inserted between the Al and substrate. The Ge insertion layer causes an increase in the initial Ge concentration in the Al. This paper investigates the effect of the Ge insertion layer. A 1-nm-thick Ge insertion layer exhibits low temperature crystallization at 275˚C and yields large grains of over 100-μm in diameter.

2. Experimental details

Amorphous Ge membranes, that is, Ge insertion layers for promoting AIC, were prepared on SiO_2 glass substrates. The thicknesses of the Ge insertion layers (defined as t_i) were 0 nm, 1 nm, 3 nm, and 10 nm. The Al layers (each being 50-nm thick) were prepared on the a-Ge membranes and then exposed to air for 10 minutes to form native Al oxide layers (AlO_x). After that, second a-Ge layers were prepared on the AlO_x layers. The total thickness of the first and second a-Ge layers was fixed to be 50 nm. All the depositions were carried out at room temperature using a radio-frequency (RF) magnetron sputtering method. The deposition rate was 23 nm/min for Ge and 25 nm/min for Al. The degree of purity for the sputtering targets was 99.99% for Ge and 99.9% for Al. Argon pressure during the sputtering was 0.2 Pa, and the RF power was set to 100 W. The samples were annealed at 275-325˚C for 0.5-100 h in a N_2 ambient to induce layer exchange growth. The growth morphologies of the samples were observed using Nomarski optical microscopy. The actual grain size and crystal orientation were evaluated using electron backscattered diffraction (EBSD) measurement. Prior to the EBSD measurement, the aluminum and oxide layers on the Ge layers were etched for one minute in an HF solution (HF: 1.5%).

3. Results and discussion

Fig. 2(a)-(d) show a typical growth evolution of the AIC-Ge, observed using Nomarski optical microscopy. These micrographs show the back surface of the sample observed through the transparent SiO_2 substrate. The thickness of the Ge insertion layer (t_i) is 1 nm and the annealing temperature (T_a) is 325˚C. The dark area indicates crystallized Ge and the bright-colored area indicates Al. The micrographs suggest that, during annealing, the Ge atoms diffuse to the back surface, grow laterally, and cover the entire surface of the substrate.

We calculated the coverage ratio of AIC-Ge to substrate for samples with and without Ge insertion (t_i: 1, 3, 10 nm) from the micrographs. The results are summarized in Fig. 2(e) as a function of the annealing time. For all samples, Ge coverage increases as the annealing time increases, and finally reaches approximately 100%. It is worth noting that a thicker Ge insertion layer corresponds to a shorter annealing time for completing AIC. This result proves that the Ge insertion layers enhance Ge supersaturation of the Al and promote growth in AIC.

Next, the nucleation time, growth velocity, grain density, and eventual grain radius were compared between samples with t_i = 0 nm, 1 nm, 3 nm, and 10 nm; and with T_a = 275˚C, 300˚C, and 325˚C. The grain size was evaluated from the micrographs as a function of annealing time. Fig. 3(a) shows the result for the sample with t_i = 1 nm and T_a = 325˚C. Grain growth starts after a certain incubation time, and then stop after several hours because of grain collisions. From Fig. 3(a), the nucleation time is estimated to be 0.9 h, the growth velocity 104 μm/h, and the eventual grain radius 267 μm. The grain density was calculated to be 450 cm^{-2} using the value of the eventual grain radius. These parameters were obtained in the same way for the other samples, and are summarized in Fig. 2(b)-(d). Fig. 2(b) clearly indicates that the nucleation time shortens with increasing t_i. We could not observe Ge nucleation for the sample annealed at 275˚C for 100 h. These results prove that the Ge insertion layer promoted Ge nucleation. On the other hand, Fig. 3(c) indicates that the growth velocity decreases with increasing t_i. The reason for this is explained later. Additionally, a higher annealing temperature provided a shorter nucleation time and a higher growth velocity for all the samples. This is simply because the Ge diffusion rate increases with an increase in the annealing temperature. Fig. 3(d) indicates that the eventual grain radius decreases with an increase in the thickness of the Ge insertion layer, while the grain density has opposite tendency. Consequently, the sample with t_i = 1 nm is optimum for simultaneously achieving growth promotion and a large grain size.

On the basis of the layer exchange mechanism, the effect of the Ge insertion is explained as follows. The expected growth mechanism is schematically shown in Fig. 3(a)-(d). Figure 3(a) shows the structure of the prepared samples. During annealing, Ge atoms in the Ge insertion layer uniformly diffuse into the Al layer, as shown in Fig. 3(b). Ge nucleation occurs as a result of supersaturation of the Al with Ge [15, 18]. Hence, a thicker t_i provides greater concentration of Ge in the Al, which results in faster nucleation because of faster supersaturation of the Al with Ge, as shown in Fig. 2(b). However, when t_i is thicker than 1 nm, the nucleation frequency is too high, as shown in Fig. 2(d). Therefore, the thickness of the Ge insertion layer has an optimum value.

After nucleation, lateral growth is induced by Ge diffusion from the top Ge layer, as shown in Fig. 3(c) [15-22, 25]. In contrast to the nucleation rate, the lateral growth rate decreased with increasing t_i, as shown in Fig. 3(c). This behavior can be explained as follows. Ge atoms diffusing from the top layer into the Al are shared by Ge crystals for lateral growth [18, 20]. Hence, the growth velocity of each grain becomes low when the grain density is high because of the thick t_i. Therefore, a role of the Ge insertion layer is to enhance Ge nucleation rather than lateral growth; the Ge insertion layer is consumed only by nucleation. A continuous supply of Ge atoms from the top Ge layer induces the completion of layer exchange through the pushing up of Al, as schematically shown in Fig 3(c) and (d) [20].

The crystal orientation was evaluated using EBSD measurement for the sample with t_i = 1 nm and T_a = 275˚C. Fig. 4(a) and (b) show crystal orientation maps in the normal direction (ND) and the transverse direction (TD) relative to the sample surface, respectively. The black solid lines indicate random grain boundaries, which were drawn based on EBSD analysis results. Fig. 4(a) indicates that the AIC-Ge layer is highly (111) oriented over the entire region. The area fraction of the (111) orientation was calculated using EBSD analysis and was found to be as high as 99%. As shown in Fig. 4(b), EBSD analysis reveals that a grain observed using Nomarski optical microscopy is divided into several different orientations. The net grain size is estimated from the TD map and is found to be over 100-μm in diameter. This value is larger than the 325˚C annealed AIC-Ge without a Ge insertion layer. Because the net grain size increases with decreasing annealing temperature [31], the enlargement of the net grain size is likely due to the low-temperature annealing (275˚C), which was accomplished by growth promotion using the Ge insertion layer.

4. Conclusions

We investigated the effects of Ge insertion below the Al layer in AIC-Ge. The Ge insertion layer promoted AIC by enhancing supersaturation of the Al with Ge, which resulted in low-temperature growth (275˚C). However, thick (≥ 3 nm) Ge insertion layers provided a high nucleation frequency and a small eventual grain size. A 1-nm-thick Ge insertion layer achieved both growth promotion and large grains of over 100 μm in diameter. Moreover, the AIC-Ge was highly (111) oriented. This low-temperature formation technique of large grained Ge (111) thin films on amorphous substrates opens up the possibility for advanced Ge-based devices on inexpensive flexible substrates.

Acknowledgements

This work was partially supported by the Murata Science Foundation and by the Casio Science Promotion Foundation. This work was performed under the Inter-University Cooperative Research Program of the Advanced Research Center of Metallic Glasses, Tohoku University.

References

[1] T. Sanada, Y. Nakakita, M. Takenaka, S. Takagi, J. Appl. Phys. 106 (2009) 073716.

[2] T. Nishimura, L. H. Lee, T. Tabata, S. K. Wang, K. Nagashio, K. Kita, A. Toriumi, Appl. Phys. Express 4 (2011) 064201.

[3] R. R. King, D. C. Low, K. M. Edmondson, C. M. Fetzer, G. S. Kinsey, H. Yoon, R. A. Sherif, N. H. Karam, Appl. Phys. Lett. 90 (2007) 183516.

[4] N. Fukata, K. Sato, M. Mitome, Y. Band, T. Sekiguchi, M. Kirkham, J. I. Hong, Z. L. Wang, R. L. Snyder, ACS Nano 4 (2010) 3807.

[5] E. P. M. Bakkers, J. Dam, S. Franceschi, L. P. Kouwenhoven, M. Kaiser, M. Verheijen, H. Wondergem, P. Sluis, Nat. Mater. 3 (2004) 769.

[6] K. Hamaya, H. Itoh, O. Nakatuka, K. Ueda, K. Yamamoto, M. Itakura, T. Taniyama, T. Ono, M. Miyao, Phys. Rev. Lett. 102 (2009) 137204.

[7] K. Toko, I. Nakao, T. Sadoh, T. Noguchi, M. Miyao, Solid-State Electron. 53 (2009) 1159.

[8] T. Sadoh, H. Kamizuru, A. Kenjo, M. Miyao, Appl. Phys. Lett. 89 (2006) 192114.

[9] J. H. Park, P. Kapur, K. C. Saraswat, H. Peng, Appl. Phys. Lett. 91 (2007) 143107.

[10] K. Toko, H. Kanno, A. Kenjo, T. Sadoh, T. Asano, M. Miyao, Appl. Phys. Lett. 91 (2007) 042111.

[11] H. Watakabe, T. Sameshima, H. Kanno, M. Miyao, Thin Solid Films 508 (2006) 315.

[12] W. Yeh, H. Chen, H. Huang, C. Hsiao, J. Jeng, Appl. Phys. Lett. 93 (2008) 094103.

[13] K. Skaike, S. Higashi, H. Murakami, S. Miyazaki, Thin Solid Films 516 (2008) 3595.

[14] M. Tada, J. H. Park, J. R. Jain, K. C. Saraswat, J. Electrochem. Soc. 156 (2009) D23.

[15] O. Nast, T. Puzzer, L.M. Koschier, A.B. Sproul, S.R. Wenham, Appl. Phys. Lett. 73 (1998) 3214.

[16] Y. Sugimoto, N. Takata, T. Hirota, K. Ikeda, F. Yoshida, H. Nakashima, H. Nakashima, Jpn. J. Appl. Phys. 44 (2005) 4770.

[17] M. Kurosawa, N. Kawabata, T. Sadoh, M. Miyao, Appl. Phys. Lett. 95 (2009) 132103.

[18] A. Sarikov, J. Schneider, J. Berghold, M. Muske, I. Sieber, S. Gall, W. Fuhs, J. Appl. Phys. 107 (2010) 114318.

[19] M. Jung, A. Okada, T. Saito, T. Suemasu, N. Usami, Appl. Phys. Express 3 (2010) 095803.

[20] B.I. Birajdar, T. Antesberger, B. Butz, M. Stutzmann, E. Spiecker, Scripta

Materialia 66 (2012) 550.

[21] A. Okada, K. Toko, K. O. Hara, N. Usami, T. Suemasu, J. Cryst. Growth 356 (2012) 65.

[22] R. Numata, K. Toko, N. Saitoh, N. Yoshizawa, N. Usami, T. Suemasu, Crystal Growth and Design 13 (2013) 1767.

[23] F. Katsuki, K. Hanafusa, M. Yonemura, T. Koyama, M. Doi, J. Appl. Phys. 89 (2001) 4643.

[24] R. Zanatta, I. Chambouleyron, J. Appl. Phys. 97 (2005) 094914.

[25] Z. M. Wang, J. Y. Wang, L. P. H. Jeurgens, F. Phillipp, E. Mittemeijer, J. Acta. Materialia 56 (2008) 5047.

[26] W. Zhang, F. Ma, T. Zhang, K. Xu, Thin Solid Films 520 (2011) 708.

[27] S. Peng, D. Hu, D. He, Appl. Surf. Sci. 258 (2012) 6003.

[28] Q. Chen, C. Li, Z. Chen, Z. Jial, M. Wu, C. Shek, C. M. L. Wu, J. K. L. Lai, Inorg. Chem. 51 (2012) 8473.

[29] M. Kurosawa, N. Kawabata, T. Sadoh, M. Miyao, ECS J. Solid State Sci. and Tech. 1 (2012) 144.

[30] K. Toko, M. Kurosawa, N. Saitoh, N. Yoshizawa, N. Usami, M. Miyao, T. Suemasu, Appl. Phys. Lett. 101 (2012) 072106.

[31] K. Toko, N. Fukata, K. Nakazawa, N. Saitoh, N. Yoshizawa, N. Usami, T. Suemasu, J. Cryst. Growth 372 (2013) 189.

Figure captions

Fig. 1. Nomarski optical micrographs of the sample with t_i = 1 nm and T_a = 325˚C. The annealing times are (a) 0.5 h, (b) 2 h, (c) 3 h, and (d) 5 h. (e) Ratio of Ge coverage to substrate as a function of annealing time, where t_i = 0 nm, 1 nm, 3 nm, and 10 nm.

Fig. 2. (a) Annealing time dependence of the sample grain radii with t_i = 1 nm and T_a = 325˚C. Insertion layer thickness (t_i) dependence of (b) nucleation time, (c) growth velocity, and (d) eventual grain radius and grain density, where T_a = 275˚C, 300˚C, and 325˚C.

Fig. 3. Schematics of the layer exchange process in AIC-Ge with a Ge insertion layer. (a) Sample structure before annealing. (b) Ge diffusion from the Ge insertion layer into the Al. (c) Ge nucleation and lateral growth induced by Ge diffusion from the top a-Ge layer, which pushes Al up into the top a-Ge layer. (d) Completion of the layer exchange.

Fig. 4. Crystal orientation of the AIC-Ge layer with t_i = 1 nm and T_a = 275˚C. EBSD images in the (a) normal direction (ND) and (b) transverse direction (TD) relative to the sample surface. The colors indicate the crystal orientation according to the inserted

color key.

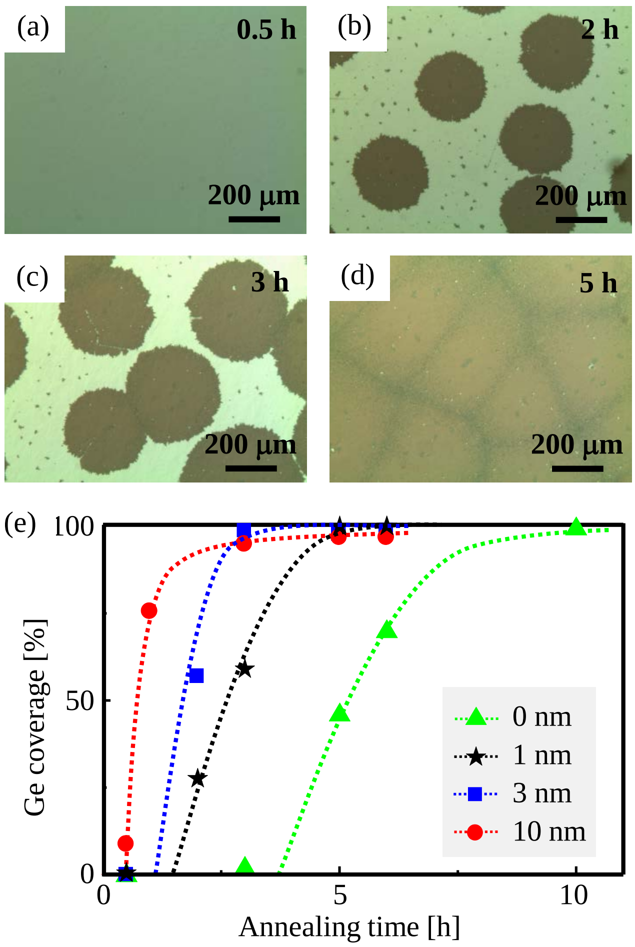
(a)
0.5 h
200 µm
(b)
2 h
200 µm
(c)
3 h
200 µm
(d)
5 h
200 µm
(e)
100
50
0
Ge coverage [%]
0
5
10
Annealing time [h]
0 nm
1 nm
3 nm
10 nm

Fig. 1

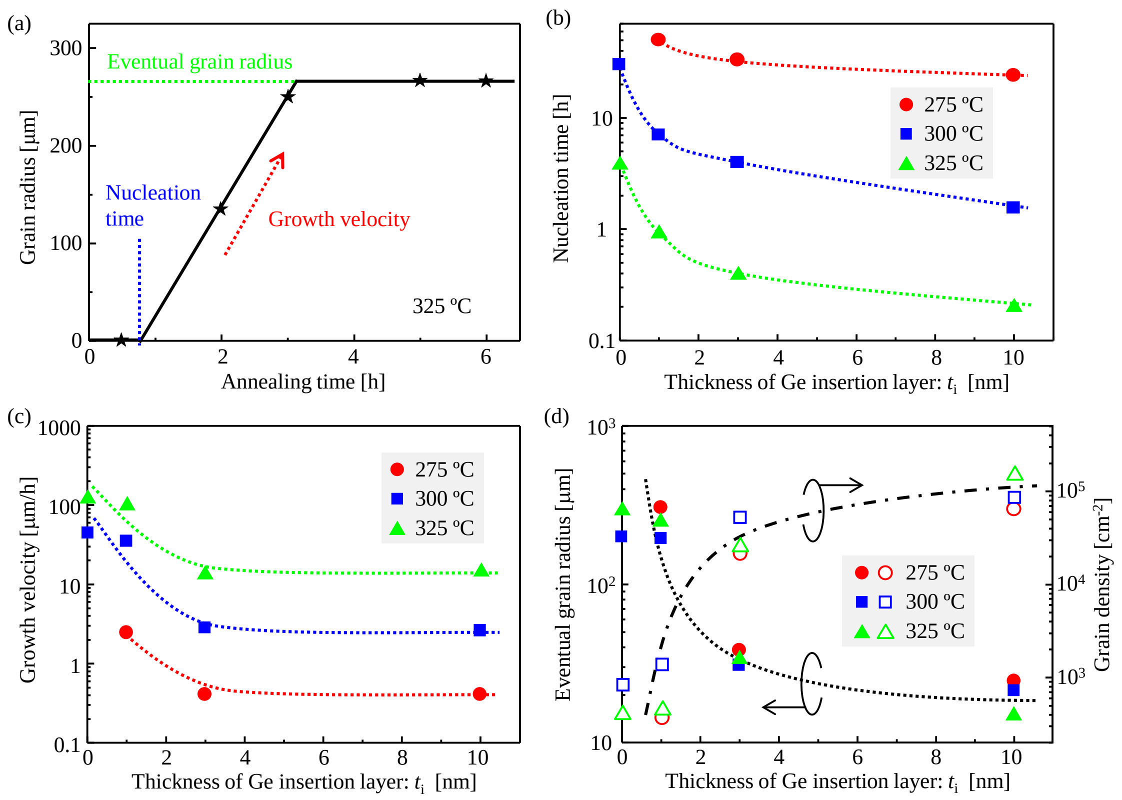
(a)
Eventual grain radius
Nucleation
time
Growth velocity
325 ºC
Grain radius [μm]
Annealing time [h]
(b)
275 ºC
300 ºC
325 ºC
Nucleation time [h]
Thickness of Ge insertion layer: t_i [nm]
(c)
275 ºC
300 ºC
325 ºC
Growth velocity [μm/h]
Thickness of Ge insertion layer: t_i [nm]
(d)
275 ºC
300 ºC
325 ºC
Eventual grain radius [μm]
Grain density [cm^{-2}]
Thickness of Ge insertion layer: t_i [nm]

Fig. 2

260

261

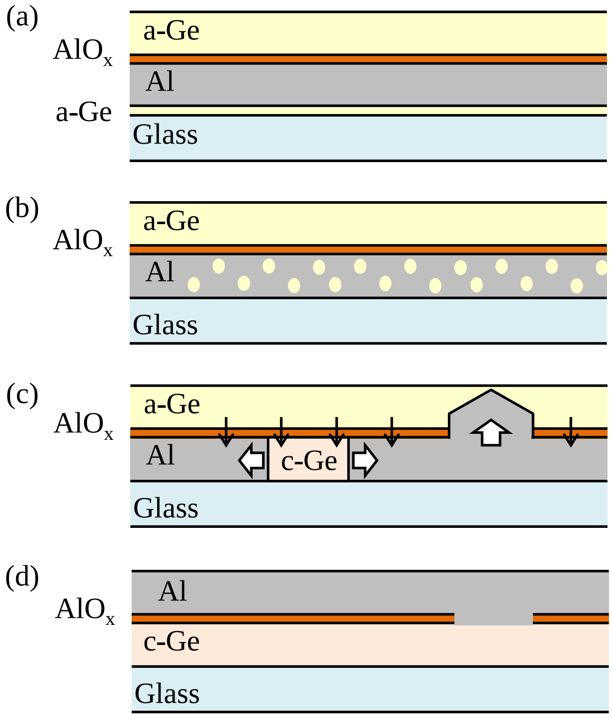
(a)
a-Ge
AlO$_x$
Al
a-Ge
Glass
(b)
a-Ge
AlO$_x$
Al
Glass
(c)
a-Ge
AlO$_x$
Al
c-Ge
Glass
(d)
Al
AlO$_x$
c-Ge
Glass

Fig. 3

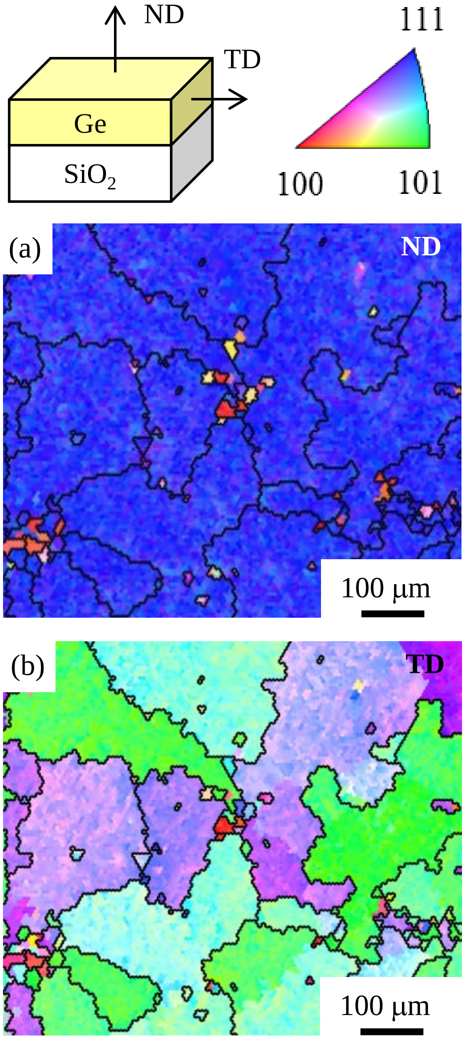

Fig. 4